Generative design of stiffened plates based on homogenization method

Ma, Xiangtao; Wang, Fayao; Aage, Niels; Tian, Kuo; Hao, Peng; Wang, Bo

Published in:
Structural and Multidisciplinary Optimization

Link to article, DOI:
10.1007/s00158-021-03070-3

Publication date:
2021

Document Version
Peer reviewed version

Generative design of stiffened plates based on homogenization method

Xiangtao Ma [a], Fayao Wang [a], Niels Aage [b], Kuo Tian [a], Peng Hao [a,*] and Bo Wang [a,*]

[a] *State Key Laboratory of Structural Analysis for Industrial Equipment, Key Laboratory of Digital Twin for Industrial Equipment, Liaoning Province, Department of Engineering Mechanics, Dalian University of Technology, Dalian, 116023, China*

[b] *Department of Mechanical Engineering, Centre for Acoustic-Mechanical Micro Systems, Technical University of Denmark, Nils Koppels Alle, Building 404, 2800 Kongens Lyngby, Denmark*

**Corresponding author: haopeng@dlut.edu.cn & wangbo@dlut.edu.cn*

Stiffened plates are widely used in aerospace structures as load-bearing components. In order to obtain the novel design of stiffened structures with good performance, a generative design method of stiffened plates (GDMSP) based on the homogenization method is proposed in this paper. It optimizes the stiffener layout based on the equivalent model. Then the detailed model can then be obtained by extracting the stiffener path from the discrete distribution of stiffener angles. Moreover, the optimized design can be obtained by size optimization based on the detailed model. Two examples are used to illustrate the proposed framework, including the stiffness maximization of the rectangle stiffener plate and the buckling load maximization of the square stiffener plate. The optimized stiffener configurations are characterized by streamlines and uniform lines, respectively. For the first example, the stiffness of the stiffener design has an improvement of 17%. For the second example, the optimized design improves the buckling load by 35%. Results indicate that the proposed method can effectively provide a novel generative design for stiffened plates. Moreover, the obtained results have a clear stiffener path and have a noticeable improvement in performance, which can be directly used to establish a detailed model.

Keywords: Generative design; Stiffened plate; Discrete material optimization; Asymptotic homogenization; Integrated optimization

1. Introduction

Stiffened plates and shells are commonly used as the load-bearing components in aerospace structures due to their high stiffness-to-weight ratio and high strength-to-weight ratio. In order to obtain the optimized design of stiffened structures with the best performance, design optimizations are generally performed. However, it is usually a difficult optimization problem, especially when the number of stiffeners is indeterminate and the stiffener layout is complicated. In the past decades, various methods have been investigated and developed from different perspectives. These methods can roughly be classified into three categories, namely topology

optimization, shape optimization, and size optimization.

The earlier works of the stiffener design are the thickness optimization of solid or shell elements. Specifically, Cheng and Olhoff [1] performed the thickness distribution optimization of rectangular and axisymmetric plates to maximize the stiffness, which is the original form of topology optimization. Chung and Lee [2] also optimized the shapes and locations of ribs with the objective of maximum stiffness using the topology optimization technique. With the development of topology optimization, many methods were developed for stiffener optimization, where the stiffener layout design is converted into the distribution optimization of material. For example, Zhou et al. [3] introduced the casting constraints to standard topology optimization and obtained the stiffener topology design, where the stiffeners are described by ordered pseudo-densities of the elements along the casting direction. Lam and Santhikumar [4] investigated the optimization of rib location under some realistic constraints. Later, Gersborg and Andreasen [5] proposed a smooth heaviside parameterization method, and Zhu et al. [6] proposed a simple method to impose the casting constraint, respectively. Liu et al. [7] additionally introduced a new set of variables based on a Heaviside-casting constraint and obtained stiffener designs with variable heights.

Moreover, Zhang and Norato [8] proposed a geometry projection topology optimization method for the stiffener layout of the plate, which requires a relatively fine mesh to capture the thickness of the plates, but this cost can be alleviated by using adaptive mesh refinement strategies [9]. And then they [10] introduced two design and manufacturing constraints relevant to the optimal rib layout problem, including the minimum separation constraint between any two ribs and the constraint of hole independence. Wang et al. [11] developed an implementation of the extrusion constraint based on the helmholtz-type anisotropic filter approach. These methods can effectively optimize the innovative stiffened topology design, but they are computationally expensive due to a large number of design variables. Especially for the practical engineering problem with large-scale, the refined stiffener topology result required that the mesh size should be less than the thickness of stiffeners, which would result in an extremely large number of design variables. Specifically, Aage et al. [12] obtained a giga-voxel computational morphogenesis design with unprecedented structural detail for the full-scale wing, which has 1.1 billion elements. Besides, Oberndorfer et al. [13] optimized practical engineering stiffened design by the ground structure approach of trusses. Ding et al. [14–16] proposed a growing and

branching tree model to perform the stiffener layout design, which is inspired by the branching system in nature. Similarly, Liu et al. [17] proposed an adaptive morphogenesis algorithm for the design of stiffened plates in a growth manner, which is inspired by the adaptive growth of leaf vein. Zhou et al. [18] developed a two-scale stiffener pattern optimization method for periodicity grid-stiffened structures. Sun et al. [19] performed the stiffener layout optimization of composite stiffened panels based on the moving morphable components method. Moreover, the stiffener designs can be obtained by topology optimization with maximum size constraints [20]. These topology optimization methods can fully explore the potential of the design domain can provide an innovative configuration design. However, topology optimization results generally require post-processing, and the shape and size optimizations based on the feature extraction configuration should be performed to obtain the final design. Because the results of topology optimization hardly meet all practical engineering requirements, such as continuous stiffeners and that the stiffeners should extend from one side to another side. Especially, it is challenging to obtain a clear stiffener path by topology optimization when the volume fraction constraint is ultra-small. As a result, most practical optimization stiffeners are limited to shape and size optimization.

For shape optimization, the mathematical functions with parameters are used to describe the path of stiffeners, and the concept of curve stiffeners and non-uniformly distribution are introduced to improve the performance of the stiffened structure. For example, Hao et al. [21] proposed a curvilinear stiffener optimization framework for the cylindrical shells with cutouts based on the spline curve. Hirschler et al. [22] performed the isogeometric shape optimization of complex stiffened multi-patch structures. Wang et al. [23] proposed a homogenization-based optimization method with linearly varying stiffener angles for curve stiffened composite structures. Kegl [24] performed the truss-stiffened shell optimization with variable thickness using the shape optimization method. Zhao and Kapania [25] investigated the buckling response of composite panels with curved stiffeners. Wang et al. [26,27] proposed a streamline stiffener path optimization method, where different stiffeners are characterized using a streamline function with different constant values. Moreover, Liu et al. [28] additionally introduced interpolation functions to describe the non-uniform distribution and variable profile of stiffeners. Hao et al. [29] performed nondeterministic optimization for curvilinear stiffened panel with multi-cutouts. Slemp et al. [30] have proved the advantages of curve stiffener design by experiment. Besides, Liu and Shimoda [31] proposed a parameter-free shape optimization method to design the shapes of stiffened thin-

walled structures for the natural vibration problem. Bojczuk and Szteleblak [32] performed the layout and shape optimization for stiffened plates. For size optimization, the structural sizes are set as the variables to determine the final design. For example, Jármai et al. [33] performed the minimum cost optimization for welded orthogonally stiffened cylindrical shells. Bushnell [34] optimized the stiffened imperfect panels under combined loads in the post-buckling regime. Wang and co-authors [35–37] performed the size optimization of stiffened shells in launch vehicles with the post-buckling regime and proposed the hierarchical stiffened shell that has low imperfection sensitivity. The results of shape and size optimization generally meet the practical requirements and can be directly used as the final design model. However, shape and size optimization limits the design space. Moreover, the number of design variables would increase sharply with the increase of stiffener number, which would bring challenges to the optimization problem. The integrated approach for multiple optimization methods can further improve the performance of structures [38]. Therefore, an integrated optimization method of stiffened plates that includes topology, shape, and size should be established. While providing innovative configuration of stiffened shell with good performance, the design provided should also have the characteristics of detailed modeling, analysis and manufacturability, which can be called as the generative design.

Based on this background, a generative design method of stiffened plates (GDMSP) based on the homogenization method is proposed in this paper, where the optimization is divided into two steps considering stiffener layout topology and structural size optimization. In the stiffener layout topology optimization, the typical stiffener cell is equivalent to the orthotropic laminate. Moreover, the multi-material topology optimization method is used to optimize the stiffener layout. Then the detailed model can be restructured according to the topology result, and the structural size optimization is performed to determine the final design. This paper is organized as follows. First, the generative design method of stiffened plates based on the homogenization method is introduced in section 2. Then, two examples of stiffness and buckling load are respectively performed to illustrate the proposed method in section 3 and 4. Finally, the findings are summarized in section 5.

2. Generative design of stiffened plates based on the homogenization method

The proposed generative design method of stiffened plates (GDMSP) based on the homogenization method can be divided into three steps, as shown in Fig. 1. The first step is to establish typical stiffener cells and obtain their equivalent material properties by the asymptotic homogenization method. The second step is to optimize the stiffener layout topology configuration based on the equivalent model, where the arrangement angles of stiffener cells are set as variables. The last step is to extract the stiffener path from the result obtained in step 2, establish the detailed model, and optimize the structural size parameters to obtain the final design that meets other requirements. In order to further illustrate the framework, each step is explained in detail in subsequent sections.

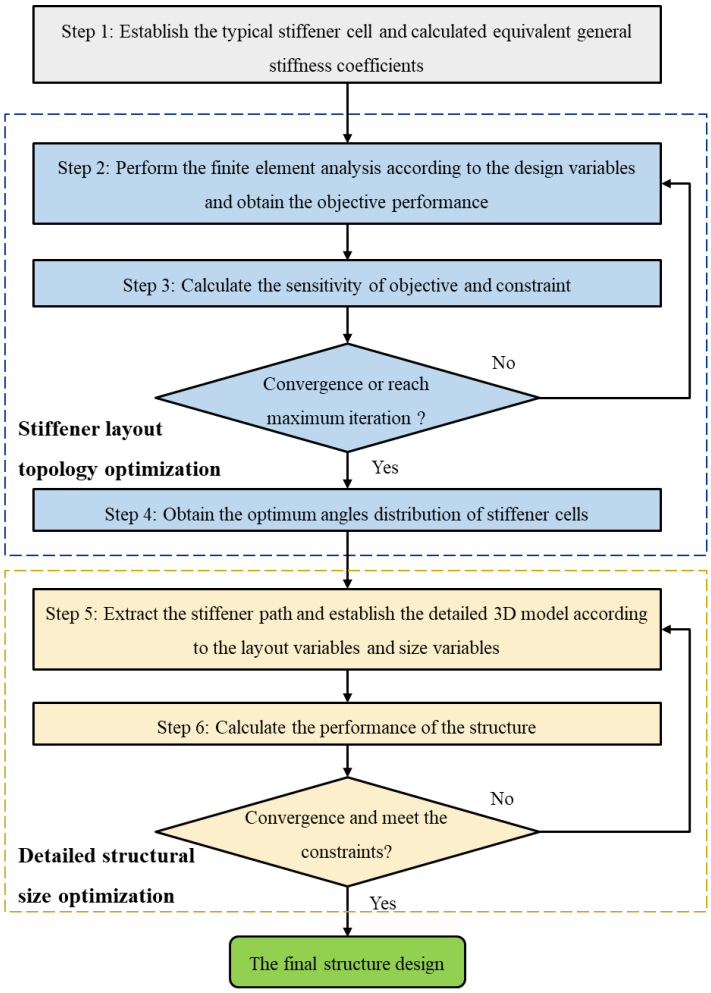

Fig. 1 Flowchart of the generative design method of stiffened plates based on the homogenization method

2.1 Asymptotic homogenization for stiffener cell

In this paper, a typical cross-reinforced stiffener cell is established in the first step, as shown in Fig. 2. The stiffener cell can be regarded as a laminate, and the equivalent laminate property can be calculated by the asymptotic homogenization (AH) method. In this paper, the AH method improved by Cheng[39] and Cai[40] is employed to calculate the equivalent general stiffness coefficients of the stiffener cell, which is briefly introduced as follows.

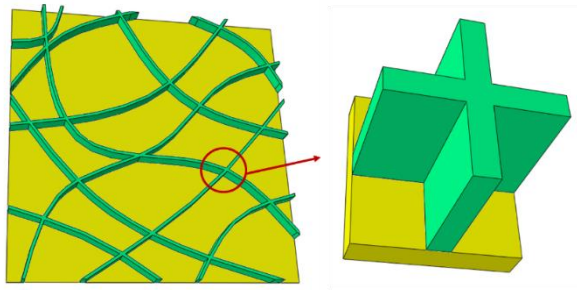

Fig. 2 Schematic diagram of the typical cross-reinforced stiffener cell

The equivalent general stiffness coefficients of the stiffener unit cell Ω include the extensional stiffness coefficients A_{ij}, coupling stiffness coefficients B_{ij}, and bending stiffness coefficients D_{ij}. They can be obtained with Eq.(1),

$$\begin{aligned} A_{ij} &= \frac{1}{|\Omega|}\int_{\Omega}\left(\boldsymbol{\varepsilon}_i^0-\boldsymbol{\varepsilon}_i^*\right)^{\mathbf{T}}\boldsymbol{C}\left(\boldsymbol{\varepsilon}_j^0-\boldsymbol{\varepsilon}_j^*\right)d\Omega \\ B_{ij} &= \frac{1}{|\Omega|}\int_{\Omega}\left(\boldsymbol{\varepsilon}_i^0-\boldsymbol{\varepsilon}_i^*\right)^{\mathbf{T}}\boldsymbol{C}\left(\bar{\boldsymbol{\varepsilon}}_j^0-\bar{\boldsymbol{\varepsilon}}_j^*\right)d\Omega \\ D_{ij} &= \frac{1}{|\Omega|}\int_{\Omega}\left(\bar{\boldsymbol{\varepsilon}}_i^0-\bar{\boldsymbol{\varepsilon}}_i^*\right)^{\mathbf{T}}\boldsymbol{C}\left(\bar{\boldsymbol{\varepsilon}}_j^0-\bar{\boldsymbol{\varepsilon}}_j^*\right)d\Omega \end{aligned} \tag{1}$$

where $\mathbf{C}$ is an elasticity matrix, subscripts *i* and *j* denote load cases ($i, j \in 1,2,6$), Ω is the domain of stiffener unit cell. The unit strain fields include three in-plane strain fields ε_i^0 and three flexural strain fields $\bar{\varepsilon}_i^0$, and the characteristic strain fields include three in-plane strain fields ε_i^* and three flexural strain fields $\bar{\varepsilon}_i^*$. Note that the unit strain fields ε_i^0 and $\bar{\varepsilon}_i^0$ can be expressed by corresponding nodal displacement fields $\boldsymbol{\chi}_i^0$ and $\bar{\boldsymbol{\chi}}_i^0$ with strain-displacement matrix $\mathbf{B}_{\boldsymbol{\varepsilon}}$ as

$$\begin{aligned}\varepsilon_i^0 &= \mathbf{B}_{\boldsymbol{\varepsilon}}\boldsymbol{\chi}_i^0 \\ \bar{\varepsilon}_i^0 &= \mathbf{B}_{\boldsymbol{\varepsilon}}\bar{\boldsymbol{\chi}}_i^0\end{aligned} \tag{2}$$

The finite element analysis is employed to obtain the reaction force vectors $\boldsymbol{f}_i$ of in-plane strain fields.

$$\boldsymbol{f}_i = \int_\Omega \mathbf{B}_{\boldsymbol{\varepsilon}}{}^T \mathbf{C}\boldsymbol{\varepsilon}_i^0 d\Omega = \int_\Omega \mathbf{B}_{\boldsymbol{\varepsilon}}{}^T \mathbf{C}\mathbf{B}_{\boldsymbol{\varepsilon}}\boldsymbol{\chi}_i^0 d\Omega = \left(\int_\Omega \mathbf{B}_{\boldsymbol{\varepsilon}}{}^T \mathbf{C}\mathbf{B}_{\boldsymbol{\varepsilon}} d\Omega\right)\boldsymbol{\chi}_i^0 = \mathbf{K}_{cell}\boldsymbol{\chi}_i^0 \tag{3}$$

Thus, the reaction force vector $\bar{\boldsymbol{f}}_i$ of the flexural strain field is $\mathbf{K}_{cell}\bar{\boldsymbol{\chi}}_i^0$. The above force vectors are applied to each node of the original finite element model, and Eq.(4) under periodic boundary conditions is solved to obtain characteristic displacements $\mathbf{a}_i^*$ and $\bar{\mathbf{a}}_i^*$.

$$\begin{aligned}\tilde{\mathbf{K}}_{cell}\mathbf{a}_i^* &= \boldsymbol{f}_i \\ \tilde{\mathbf{K}}_{cell}\bar{\mathbf{a}}_i^* &= \bar{\boldsymbol{f}}_i\end{aligned} \tag{4}$$

where $\tilde{\mathbf{K}}_{cell}$ is the stiffness matrix of the stiffener cell under the periodic boundary condition. The characteristic strain fields $\boldsymbol{\varepsilon}_i^*$ and $\bar{\boldsymbol{\varepsilon}}_i^*$ can also be expressed by corresponding characteristic displacement fields $\mathbf{a}_i^*$ and $\bar{\mathbf{a}}_i^*$ with strain-displacement matrix $\mathbf{B}_{\boldsymbol{\varepsilon}}$ as

$$\begin{aligned}\boldsymbol{\varepsilon}_i^* &= \mathbf{B}_{\boldsymbol{\varepsilon}}\mathbf{a}_i^* \\ \bar{\boldsymbol{\varepsilon}}_i^* &= \mathbf{B}_{\boldsymbol{\varepsilon}}\bar{\mathbf{a}}_i^*\end{aligned} \tag{5}$$

Therefore, the general stiffness coefficients of the stiffener cell can be obtained by Eq.(6), namely

$$\begin{aligned}\mathrm{A}_{ij} &= \frac{1}{|\Omega|}\left(\boldsymbol{\chi}_i^0 - \mathbf{a}_i^*\right)^{\mathbf{T}} \mathbf{K}_{cell}\left(\boldsymbol{\chi}_j^0 - \mathbf{a}_j^*\right) \\ \mathrm{B}_{ij} &= \frac{1}{|\Omega|}\left(\boldsymbol{\chi}_i^0 - \mathbf{a}_i^*\right)^{\mathbf{T}} \mathbf{K}_{cell}\left(\bar{\boldsymbol{\chi}}_j^0 - \bar{\mathbf{a}}_j^*\right) \\ \mathrm{D}_{ij} &= \frac{1}{|\Omega|}\left(\bar{\boldsymbol{\chi}}_i^0 - \bar{\mathbf{a}}_i^*\right)^{\mathbf{T}} \mathbf{K}_{cell}\left(\bar{\boldsymbol{\chi}}_j^0 - \bar{\mathbf{a}}_j^*\right)\end{aligned} \tag{6}$$

In this way, the stiffener cell is equivalent to an orthotropic laminate. Moreover, the stiffener layout design is converted into the principal direction optimization of laminates, which is more straightforward than conventional topology optimization for stiffener layout. Furthermore, the computational cost of optimization can be significantly reduced since the number of elements has been drastically reduced.

2.2 Topology optimization of stiffener layout

The stiffener layout design has been converted into the principal direction optimization of laminates. When various stiffener cells with different arrangement angles are regarded as different materials, this problem can be

solved by multi-material topology optimization methods, such as the discrete material optimization (DMO) method [41–43], shape function with penalization (SFP) method [44] and binary coded parameterization (BCP) method [45], etc. Particularly, the DMO method is employed in this paper, which is briefly introduced with the stiffness objective as follows.

Firstly, a candidate material set should be assembled, where each candidate material represents one arrangement angle of stiffener cell, i.e., corresponding equivalent material property (ABD matrix). For the cross-reinforced stiffener cell, a candidate material set with 15 degrees separation is selected. Due to the symmetry of the cross-reinforced stiffener cell, there are six candidate materials, as shown in Fig. 3.

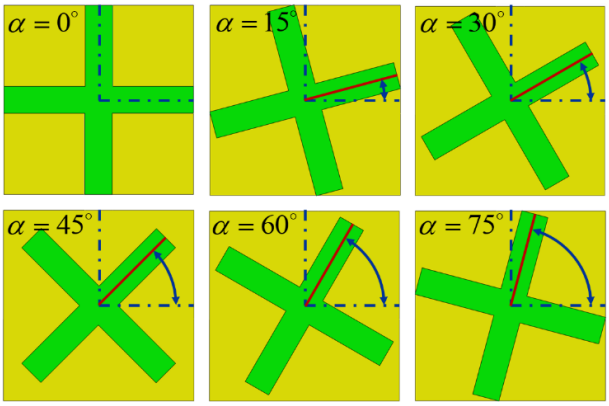

Fig. 3 Schematic diagram of six candidate materials of the cross-reinforced stiffener cell

Then, a 3D plate model without stiffeners is established and meshed, where each element represents one cross-reinforced stiffener cell with a given candidate angle. Next, the DMO is used to achieve the appropriate angle selection of stiffener cells for all elements of the plate. In the optimization process, the constitutive properties of each element are calculated by weighted summation of all candidate constitutive matrices. Consequently, instead of the arrangement angle of the stiffener cell, the variables are pseudo-densities that are used to calculate the weights of the candidate materials for all elements. The number of design variables is the product of the number of elements and the number of candidate materials. For an example with m candidate materials and n elements, the variables are $\{x_{11}, x_{12}...x_{1m}; x_{21}, x_{22}, x_{2m}; ...; x_{n1}, x_{n2}, x_{nm}\}$, where x_{nm} stands for the pseudo-density of the m^{th} candidate material for the n^{th} element. The objective of DMO is to make one of the variables be 1.0 and the others to be 0.0 for every element, indicating that one distinct candidate material is

chosen, thereby achieving discrete material optimized design. The optimization formulation for stiffness maximization can be expressed as follow,

$$\begin{aligned} &\min_{x} : \mathbf{F}^{\mathrm{T}}\mathbf{U} = \mathbf{U}^{\mathrm{T}}\mathbf{K}\mathbf{U} \\ &\text{subject to}: \mathbf{K}\mathbf{U} = \mathbf{F} \\ &\qquad 0.0 \le \underline{x} \le x_{ij} \le 1.0, \quad i = 1,...,n, \quad j = 1,...,m \end{aligned} \tag{7}$$

where $\mathbf{U}$ and $\mathbf{F}$ are the global displacement and force vectors, respectively, $\mathbf{K}$ is the global stiffness matrix, x_{ij} is the variable, and *i* and *j* are the number of elements and candidate materials. In the process of DMO, the geometry and mesh are fixed, and only the material is changed. To obtain a distinct choice of material, a penalty interpolation function is used, which is effective in weakening the stiffness of elements with intermediate value. The constitutive matrix of the element $\boldsymbol{C}_i^{\,e}$ can be calculated as

$$\boldsymbol{C}_i^{\,e} = \sum_{j=1}^{m} w_{ij}\boldsymbol{C}_j = w_{i1}\boldsymbol{C}_1 + w_{i2}\boldsymbol{C}_2 + \cdots + w_{im}\boldsymbol{C}_m, \quad 0 \le w_{ij} \le 1 \tag{8}$$

where $\boldsymbol{C}_j$ is the constitutive matrix of the j^{th} candidate material (i.e., the equivalent ABD matrix of stiffener cell with given angle). Each weight function w_{ij} should be valued between 0 and 1 to be physically allowable. And the weights are calculated with variables as

$$w_{ij} = \left(x_{ij}\right)^{p} \prod_{k=1;k\neq j}^{m} \left(1-\left(x_{ik}\right)^{p}\right) \quad j = 1,...,m \tag{9}$$

where the generalized solid isotropic material penalization strategy with the penalty term $\left(1-x_{ik}\right)_{k\neq j}$ is adopted, aiming at pushing the variables x_{ij} towards being either 0.0 or 1.0. Besides, it is necessary to make the sum of variables of one element equal to 1.0 (i.e. $\sum_{j=1}^{m} x_{ij} = 1.0$). Otherwise, physically meaningless results containing many intermediate variables may be obtained. It should be noted that a series of linear inequality constraints are imposed to ensure that the above equality constraints are approximately satisfied in this paper as

$$0.99 < \sum_{j=1}^{m} x_{ij} < 1.0 \tag{10}$$

Moreover, the sensitivities are calculated with Eq.(11), and the optimization problem is solved with the

Method of Moving Asymptotes (MMA) proposed by Svanberg [46].

$$\frac{\partial \mathrm{C}}{\partial x_{ij}} = -(\mathbf{u}_i^e)^{\mathrm{T}} \frac{\partial \mathbf{K}_i^e}{\partial x_{ij}} \mathbf{u}_i^e, \ i = 1, 2, 3, ..., n \tag{11}$$

To ensure that all candidate materials are treated equally, the initial values of the design variables are set as uniform, i.e., $x_{ij} = \frac{1}{m}$ for all elements. The optimization iteration loop is stopped when variables show no further obvious change or the maximum number of loops is reached. Afterward, the distinct choice of candidate material can be obtained by enforcing the variables to 1.0 or 0.0 according to the optimized result. It aims at eliminating intermediate values. The intermediate value is a common phenomenon in topology optimization [42,43,47]. However, the intermediate values have no physical meaning for DMO. In this paper, the highest variable value of each element is put to 1.0 and other variables are forced to 0.0. Finally, a complete 0-1 topology optimization solution representing the angle distribution of the stiffener cell is obtained.

2.3 Stiffener path extraction for detailed modeling

Because the distribution of stiffener cells does not strictly meet the periodicity assumption in the homogenization theory, the equivalent stiffness coefficients cannot accurately represent the performance of the real cell. Therefore, the optimized results using the homogenization-based model generally have errors compared with the real structures. Moreover, the mass of the structure does not change in the process of optimization because the mass of stiffener cells with different angles are the same. However, the mass of the detailed 3D model is different because the stiffener length would change during the extraction process, which results in a change in stiffener mass. Besides, the optimized result obtained by DMO is a discrete angle distribution of stiffener cells. In order to obtain optimized designs with the mass constraint, the stiffener path should be extracted based on the discrete distribution of angles, and the structural size optimization based on the detailed model should be carried out.

In this paper, the stiffener path extraction (stiffener cell angle continuity) was performed by the fitting function method. At first, the optimized distribution of discrete angles for stiffener cells is split into groups where the discrete angles are orthogonal to each other. Then the direction gradients of all elements can be calculated for different groups. Next, the stiffener paths can be characterized by the fitting function method. In

this paper, the stiffener path is characterized by the streamlines. Specifically, based on seeds uniformly arranged on edges, the corresponding streamlines along the direction gradients can be described and obtained according to the Eq.(12)-(15).

$$(x^i_0, y^i_0) = (sx^i, sy^i),\ (i = 1, 2, ..., k) \tag{12}$$

$$\bar{y}^i_{n+1} = y^i_n + hf'(x^i_n, y^i_n) \tag{13}$$

$$y^i_{n+1} = y^i_n + \frac{h}{2}[f'(x^i_n, y^i_n) + f'(x^i_{n+1}, \bar{y}^i_{n+1})],\ y^i_n \in [y_{\min}, y_{\max}] \tag{14}$$

$$x^i_{n+1} = x^i_n + h,\ x^i_n \in [x_{\min}, x_{\max}] \tag{15}$$

where sx^i and sy^i are coordinates of seeds on edges, k is the number of seeds, x^i_n and y^i_n are coordinates of the n^{th} nodes on streamline started from the i^{th} seed, $\bar{y}^i_{n+1}$ is the predicted value of y^i_n, f' is the gradient field of orientations, and h is the iteration step for calculating the path, $x_{\min}$, $x_{\max}$, $y_{\min}$ and $y_{\max}$ are the boundaries of coordinates. Then, the extracted stiffener path can be obtained by combing all groups. Finally, the detailed 3D finite element model can be established with spline curves and analyzed using commercial finite element software. The schematic process is shown in Fig. 4, where ten seeds are arranged on the top edge of group 1, five seeds are arranged on the right edge, and ten seeds are arranged on the lower edge of group 2. Now, the stiffener path can be extracted, categorized, and features simplified to meet more common manufacturing techniques.

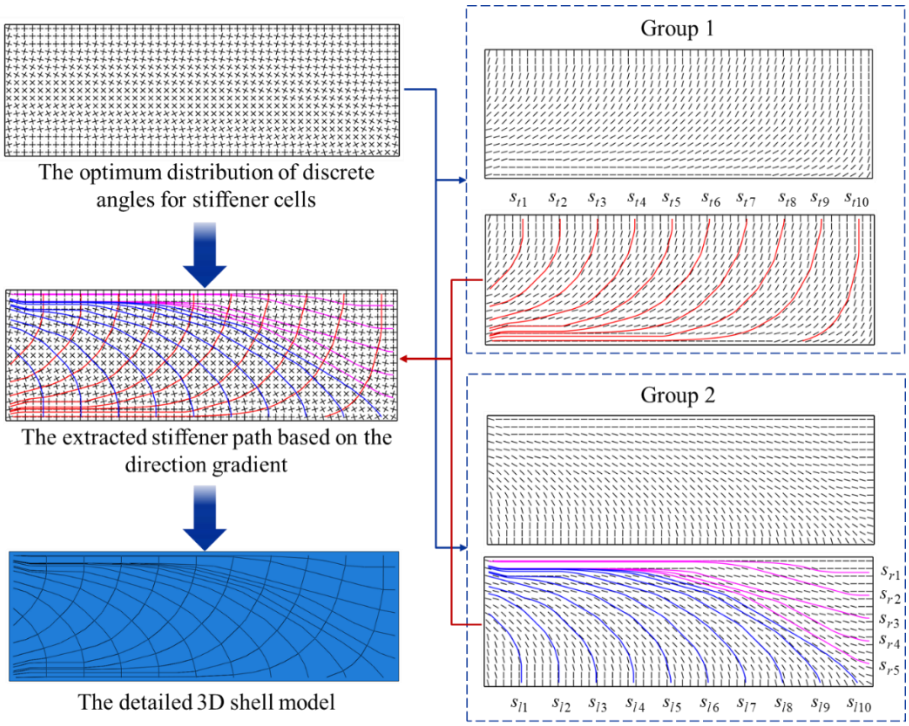

Fig. 4 The flowchart of stiffener path extraction and detained modeling

3. Stiffness maximization of rectangle stiffener plate with distributed load

In this section, a stiffness maximization example for a rectangular stiffener plate under uniform load is used to illustrate the proposed method. The length of the rectangular plate a is 300 mm, and the width b is 100 mm. The material is aluminum alloy, its elasticity modulus is 70000 MPa, its density is 2.7×10^{-6} kg/mm^3, and its Poisson's ratio is 0.3. The mesh is fixed with 850 (50×17) four-node shell finite elements in the discrete material optimization process. The left edge is fixed and a 10 N/mm uniform distributed load is applied on the top edge, as shown in Fig. 5.

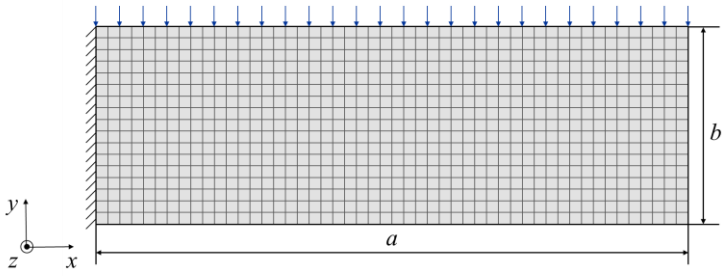

Fig. 5 Schematic diagram of rectangle plate with mesh, boundary and load

3.1 Discrete material optimization based on the equivalent material property of stiffener cells

The typical cross-reinforced stiffener cell with solid elements is established first. The size of the stiffener cell is determined as 5 mm, which is a little smaller than the mesh size in DMO. Moreover, the mesh size in the stiffener cell is set at 0.125 mm, result in 64000 solid elements in total, as shown in Fig. 6. Then, the periodic boundary is applied to its outer surfaces in the in-plane directions, and the equivalent material property (ABD matrix) of the stiffener cell can be obtained by the asymptotic homogenization method, wherein the green skin region and yellow stiffener region are given solid material, and the gray region is given void material (solid material properties scaled by 10e-7). The equivalent general stiffness coefficients are listed in Table 1. It should be pointed out that the sizes of the stiffener cell do not have to strictly match the stiffener size and mesh size of the real structure because the sizes of stiffeners and skins will change in the detailed optimization stage. When the basic configuration of the stiffener cell does not change, the same distribution of angles would be obtained even if the cell size is proportionally enlarged or reduced. Moreover, the change of relative size of skin and stiffener in the unit cell only slightly influences optimization results. It is recommended that the proper ratio of the size for skin and stiffeners be ensured so that the skin and stiffeners significantly contribute to the equivalent stiffness.

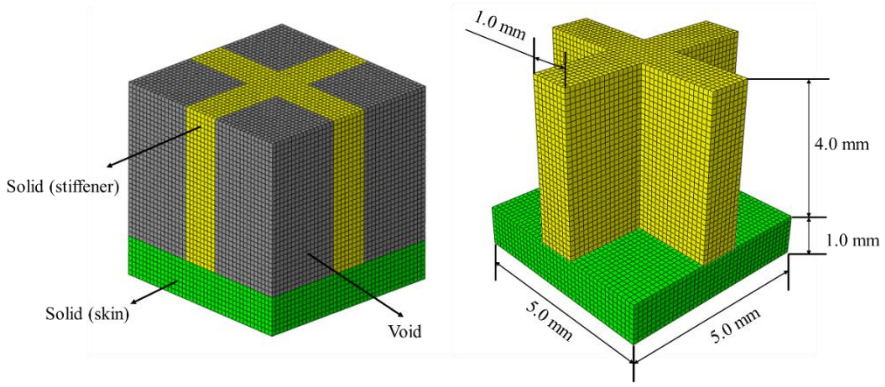

Fig. 6 The size and mesh of typical cross-reinforced stiffener cell for asymptotic homogenization

Table 1 The equivalent general stiffness coefficients of the stiffener cell with 5 mm length

A_{11}	A_{12}	A_{13}	A_{21}	A_{22}	A_{23}	A_{31}	A_{32}	A_{33}
1.37e5	2.76e4	1.80e-9	2.76e4	1.37e5	1.59e-9	1.83e-9	1.61e-9	3.04e4
B_{11}	B_{12}	B_{13}	B_{21}	B_{22}	B_{23}	B_{31}	B_{32}	B_{33}
-4.00e5	-1.00e5	-4.50e-9	-1.00e5	-4.00e5	-4.07e-9	-4.44e-9	-3.63e-9	-1.16e5
D_{11}	D_{12}	D_{13}	D_{21}	D_{22}	D_{23}	D_{31}	D_{32}	D_{33}
1.46e6	3.92e5	1.83e-8	3.92e5	1.46e6	2.36e-8	2.03e-8	1.84e-8	4.61e5

As for stiffener cells with other angles, the equivalent material property can easily be calculated with Eq.(16)-(17). In this paper, the candidate material set consists of six candidate material, as shown in Fig. 3.

$$\begin{aligned} \mathbf{A}_\alpha &= \mathbf{T}_\alpha^T \mathbf{A} \mathbf{T}_\alpha \\ \mathbf{B}_\alpha &= \mathbf{T}_\alpha^T \mathbf{B} \mathbf{T}_\alpha \\ \mathbf{D}_\alpha &= \mathbf{T}_\alpha^T \mathbf{D} \mathbf{T}_\alpha \end{aligned} \tag{16}$$

$$\mathbf{T}_\alpha = \begin{bmatrix} \cos^2(\alpha) & \sin^2(\alpha) & 2\cos(\alpha)\sin(\alpha) \\ \sin^2(\alpha) & \cos^2(\alpha) & -2\cos(\alpha)\sin(\alpha) \\ -\cos(\alpha)\sin(\alpha) & \cos(\alpha)\sin(\alpha) & \cos^2(\alpha)-\sin^2(\alpha) \end{bmatrix} \tag{17}$$

Next, the DMO is performed to optimize the stiffener layout. The objective is to minimize the strain energy, and the optimization formula is as given in Eq.(7). For this example, each element has six variables, resulting in 5100 variables in total. Moreover, the penalty value is set to 1.0 to reduce the nonlinearity of the optimization problem, and the optimization process terminates when the maximum change of variables is less than 0.001 or the iteration reaches 100. At last, the optimized discrete angles distribution of stiffener cells can be obtained, as shown in Fig. 7, and the DMO iteration history curve is shown in Fig. 8. It can be seen that the stiffeners naturally extend from other edges to the fixed edge, and the stiffeners near the loading side are along the direction of the distributed load. Most of the stiffener cells in the middle area are oriented by 45 degrees, which makes the internal force transmission to surrounding areas as high as possible.

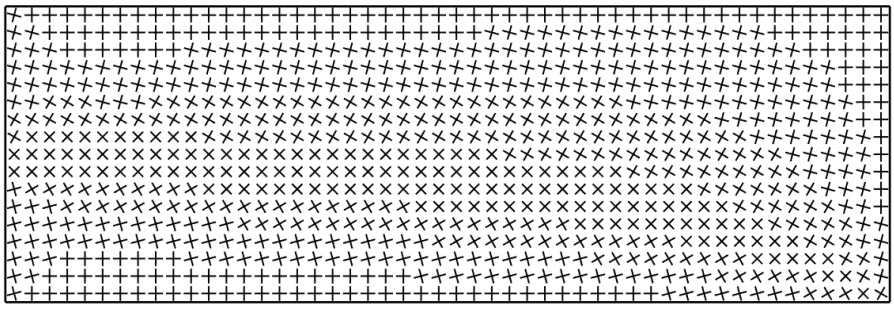

Fig. 7 The optimized discrete angle distribution of stiffener cells obtained by DMO for stiffness optimization of the rectangle stiffener plate

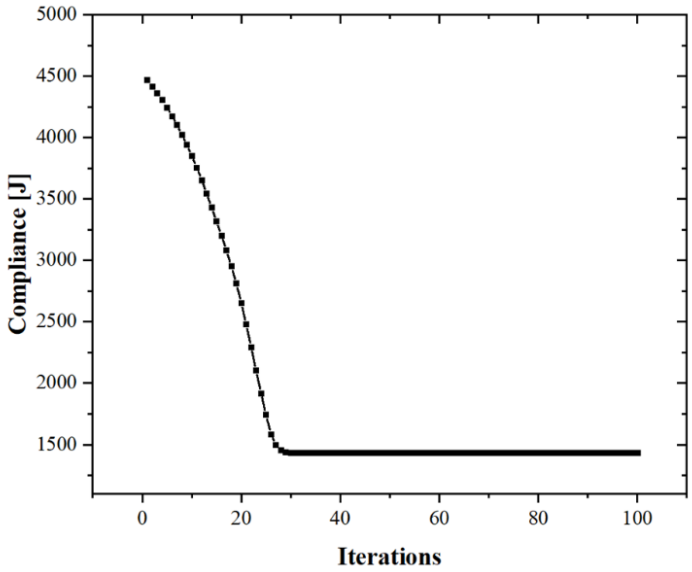

Fig. 8 The DMO iteration history curve of compliance optimization for the rectangle stiffener plate

Now the detailed 3D model can be established for comparison. For the optimized stiffener layout configuration, the number of the seeds on the top, the right and the lower edges are set as 50, 17, and 50, respectively. Then a dense stiffener path can be obtained, as shown in Fig. 9. For the initial orthogonal configuration, the number of transverse stiffeners and the number of longitudinal stiffeners are set as 17 and 50. Their structural sizes are consistent with the size of the stiffener cell, i.e., the thickness of the skin, the height and thickness of stiffeners are set as 1.0 mm, 4.0 mm, and 1.0 mm, respectively. Now the detailed 3D models can be established and analyzed in commercial finite element software. Besides, it should be pointed out that the seeds are arranged at the center coordinates of elements closest to the edges, not the nodes on the edges in

this paper. Therefore, the stiffeners do not extend to actual edges, and there is a gap between stiffeners and edges. However, the stiffeners extend to edges can be obtained by interpolating the unit cell angle of the elements to the nodes and placing seeds on the edge/margin nodes, which is not difficult.

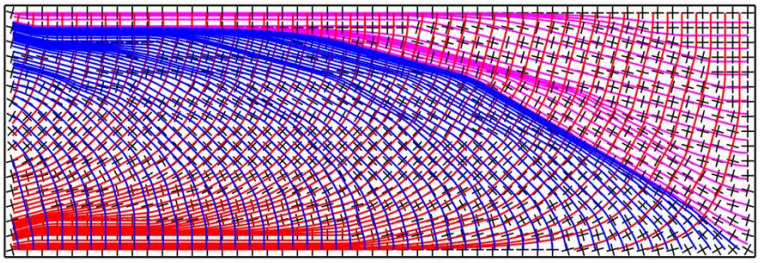

Fig. 9 The densest stiffener path extracted from the optimized discrete angle distribution of stiffener cells

In this paper, the 3D shell models are reconstructed in ABAQUS. The element type is selected as S3, the mesh size is set to 0.5 mm, and a linear static analysis is used to calculate the strain energy of the structures. The detailed models and their deformation fields under the distributed load are shown in Fig. 10. It can be seen that the structural design is improved by changing the stiffener layout. Specifically, the strain energy of the detailed models for the initial design and the optimized design are 939.31 J and 591.12 J, respectively. The stiffness of the detailed design has an improvement of 58.90% compared with the initial design, and the mass of the detailed initial design (0.21 kg) is 10.53% higher than that of the initial design (0.19 kg). However, it should be pointed out that there are errors between the equivalent model and the detailed model. The strain energy of the equivalent model of the optimized result by DMO is 1436.40 J. The reason for the error is mainly caused by the following aspects, 1) the stiffener cells do not strictly meet the periodic boundary conditions, especially in the out-of-plane direction without unit cell repetition. 2) the type of elements used in the equivalent model and detailed model is different. Nevertheless, this does not affect the conceptual layout and primary stiffener path provided by DMO for the subsequent optimization. In addition, some constraints need to be considered based on conceptual design in engineering applications, which may result in the final detailed design fail to achieve the significant improvement in performance as in the theoretical and conceptual design stage. Therefore, it is necessary to perform detailed modeling and analysis based on the conceptual design in practical engineering applications. To alleviate this shortcoming, size optimization based on the detailed model is carried out in the next section. Moreover, there would be an inconsistency between the stiffener layout obtained by

DMO and the post-process design after structural size optimization due to the change of seed parameters.

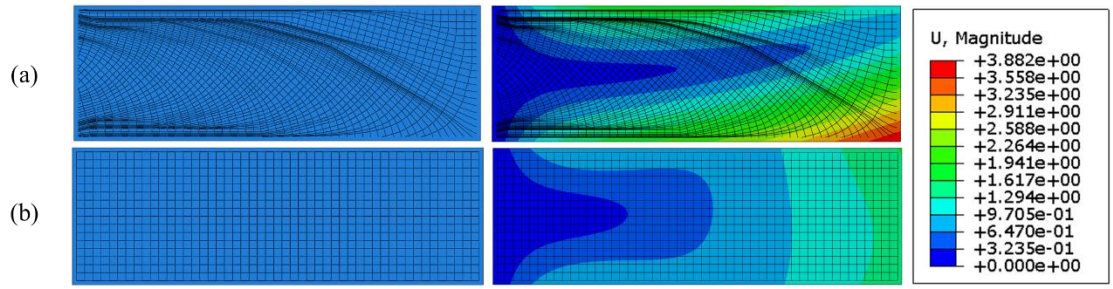

Fig. 10 The structure models and deformation fields under the distributed load, (a) the optimized stiffener layout design, (b) the traditional orthogonal configuration stiffener design

3.2 Structural size optimization based on the detailed model

In order to make a fair comparison, size optimization of the initial configuration and the optimized stiffener layout is carried out under a mass constraint. In the size optimization process, the design variables contain both discrete layout variables and continuous size variables. For the optimized stiffener layout, there are three discrete layout variables s_t, s_r and s_l that denote the number of seeds on the three edges. For the orthogonal configuration, there are two discrete layout variables n_{ts} and n_{ls} that denote the number of transverse stiffeners and longitudinal stiffeners. Moreover, they all have two continuous size variables $h_{stiffener}$ and $t_{stiffener}$ that represent the height and thickness of the stiffeners, respectively. In order to investigate the influence of the stiffener layout, the thickness of the skin t_{skin} is set to a constant of 1.00 mm in this section. The optimization formula is as shown in Eq.(18),

$$\begin{aligned} \min_{X} &: \mathbf{F}^{\mathrm{T}}\mathbf{U} = \mathbf{U}^{\mathrm{T}}\mathbf{K}\mathbf{U} \\ \text{subject to} &: \mathbf{K}\mathbf{U} = \mathbf{F} \\ & M \le \overline{M} \\ & \underline{X_d} \le X_d \le \overline{X_d} \\ & \underline{X_c} \le X_c \le \overline{X_c} \end{aligned} \tag{18}$$

where the X_d is the discrete variables, X_c is the continuous variables. M is the total mass of the structure and $\overline{M}$ is the mass constraint. It should be pointed out that the detailed model is established using a 3D shell model in ABAQUS. The element type is selected as S3, mesh size is determined as 0.5 mm, and a linear static analysis is used. In order to search for the optimum solution, the hybrid optimization

strategy is implemented. Specifically, the Multi-island Genetic algorithm [48] is employed at first, wherein the sub-population size is set at 200, the number of islands is set at 2, and the number of generations is set at 20. Then the gradient-based Sequential Quadratic Programming-NLPQL [49] algorithm is used to find the local optimum solution wherein the result of the genetic algorithm is set as the initial solution. In this way, the optimized structural design can be obtained. Due to the premature convergence of genetic algorithm optimization, the genetic optimization process is manually stopped, and a total of 2141 analyses based on detailed finite element models are performed. With the addition of 40 iterations of gradient optimization, 2181 analyses are performed for the whole hybrid optimization process, which takes about 325 hours. It is noted that most of time is spent on modeling and meshing of detailed finite element model. Moreover, all analysis and optimization in this paper were carried out using a computer server with Intel(R) Xeon(R) CPU E5-2670 v3 @ 2.30GHz and 128GB RAM. For comparison, the upper limits, the lower limits, the mass constraint, and the optimized design parameters of variables are listed in Table 2 and Table 3. In addition, their structural models and deformation fields under a distributed load are shown in Fig. 11.

Table 2 The upper limits, the lower limits, the mass constraint and optimized design parameters of variables of the optimized stiffener layout design for minimization strain energy

	s_t	s_r	s_l	t_{skin} [mm]	$h_{stiffener}$ [mm]	$t_{stiffener}$ [mm]	M [kg]	Strain energy [J]
Lower limit of variables	0	0	0	1.00	2.00	0.50	-	-
Upper limit of variables	20	6	20	1.00	10.00	2.00	0.13	-
Optimized design parameters	20	3	17	1.00	2.00	1.17	0.13	**791.24**

Table 3 The upper limits, the lower limits, the mass constraint and optimized design parameters of variables of the traditional orthogonal configuration for minimization strain energy

	n_{ts}	n_{ls}	t_{skin} [mm]	$h_{stiffener}$ [mm]	$t_{stiffener}$ [mm]	M [kg]	Strain energy [J]
Lower limit of variables	2	2	1.00	2.00	0.50	-	-
Upper limit of variables	45	45	1.00	10.00	2.00	0.13	-
Optimized design parameters	17	2	1.00	2.00	1.75	0.13	925.79

It is found that the stiffness of the optimized stiffener layout design has an improvement of 17.00%

compared with the traditional orthogonal configuration with the same mass. Moreover, it can be seen from Fig. 11 that the optimized stiffener configuration significantly improves the deformation pattern of the structure by changing the stiffener layout. Especially, although the maximum displacement of the stiffened plate with orthogonal configuration is relatively small, its deformation mode is a local form. In contrast, the deformation mode of the innovative stiffened configuration is more global, which obviously has a gradually spreading pattern from the fixed left boundary to the right side. Furthermore, for the orthogonal configuration, there is no longitudinal stiffener (only two longitudinal stiffeners on the left and right sides, corresponding to the lower bound of variable for the number of stiffeners), which indicates that the vertical stiffeners are insignificant for the rectangle plate under a distributed load on the top edge. Besides, it is found that the stiffener height of both designs is the lower bound of the design variable, which illustrates that the stiffeners have little contribution to the stiffness of plates. This is because the stiffeners provide bending stiffness, and the optimum design for maximum stiffness under uniform load in the plane should have no stiffeners and only have skin. It is consistent with the conclusion that the optimum microstructure is an isotropic solid material when only considering stiffness in Ref.[50].

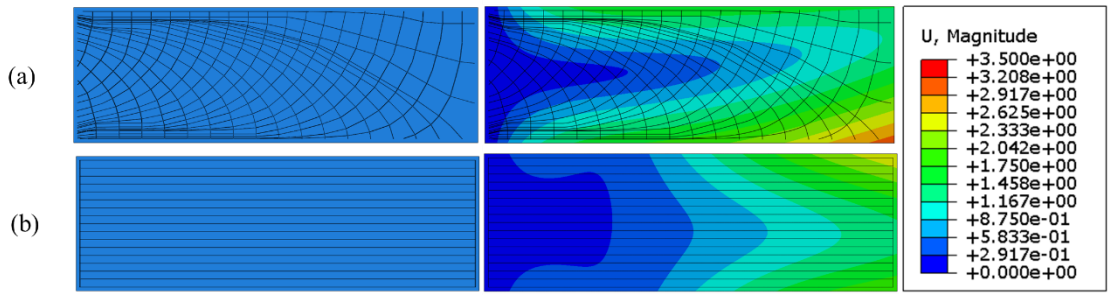

Fig. 11 The structure models after the structural size optimization and corresponding deformation fields under the distributed load, (a) the optimized stiffener layout design, (b) the traditional orthogonal configuration stiffener design

Furthermore, the influence of mesh dependency on the optimized results is investigated. The layout design variables and size variables are fixed, as given in Table 2, but the mesh for DMO is changed. The strain energy, the mass, and the deformation fields of the detailed model of the optimized result with different meshes are listed in Table 4. It is found that all designs have almost the same stiffener configuration and the same mass,

but at the same time that their stiffness increases as the mesh is refined. Especially the distance between the stiffeners and the edges would increase as the mesh size increase, which mainly leads to the decrease of structural stiffness. Because the path of the stiffeners is described based on the center coordinates of mesh. Besides, it should be noted that when the mesh size is too large, the obtained detailed stiffener layout design may be distorted due to insufficient gradient information describing the stiffener path. Therefore, it is recommended that the mesh should be refined enough in the step of stiffener layout topology optimization, which could ensure that the extracted stiffener path is closer to the optimized stiffener layout. Besides, it is noted that the kind of stiffener configuration produced by the proposed method is complex to manufacture, which can be concurrently be manufactured with processes such as additive manufacturing milling and casting. The stiffeners path should be further extracted manually or some manufacturing constraints should be introduced in the following works from a practical perspective.

Table 4 The strain energy, the mass and the deformation fields of the detailed model of the optimized result with different mesh

Mesh size	Strain energy [J]	*M* [kg]	Improvement of stiffness compared with the traditional orthogonal design	Deformation fields
75×25	767.18	0.13	20.67%	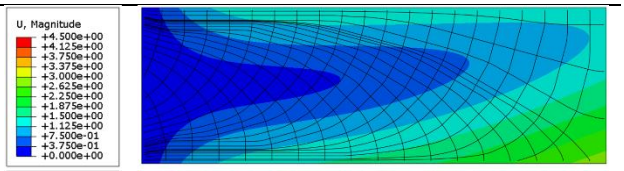
60×20	778.01	0.13	19.00%	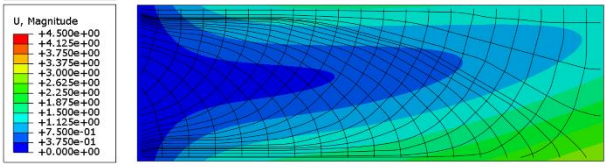
50×17	791.24	0.13	17.00%	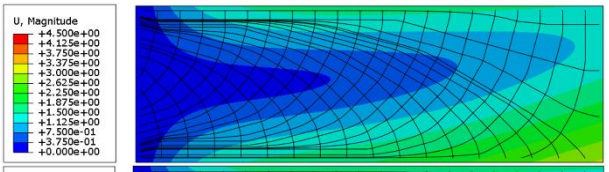
43×14	801.59	0.13	15.49%	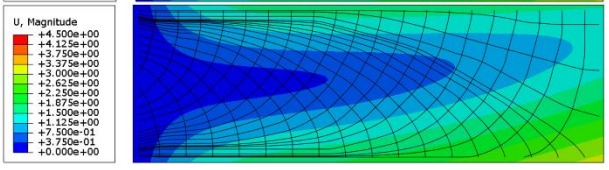

38×13	820.09	0.13	12.89%	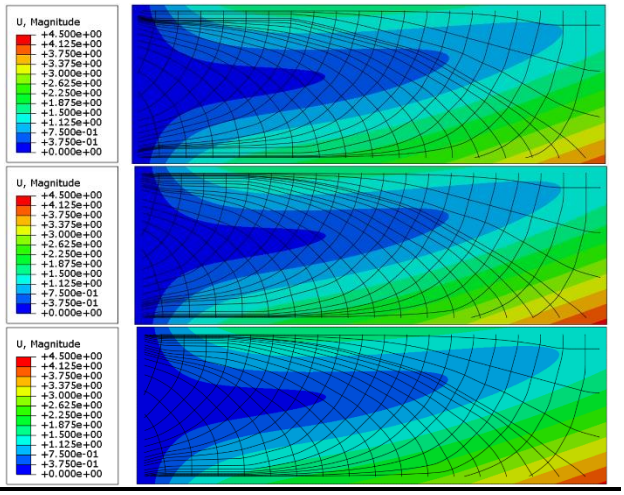
33×11	826.71	0.13	11.98%	
30×10	833.28	0.13	11.10%	

Besides, the SIMP (Solid Isotropic Material Penalization) topology optimization method with Demold constraint and size control is performed to obtain the stiffener layout design in ABAQUS [42]. A solid finite element model is used with element type C3D8R. The mesh size is set at 0.5 mm, which results in 682176 elements in total. The skin region is set as a frozen area, and the Demold constraint is applied to the normal direction of the skin. The thickness of the skin is 1.0 mm, and the design domain of the stiffener is 2.0 mm. There are four solid elements in the height direction of the design domain for stiffeners. According to the optimized result in Table 2 and Table 3, the mass of stiffeners is 0.049 kg, accounting for 37.70% of the total mass. For comparison, the upper limit of volume fraction is set as 30.26%, which would make the ratio of the stiffeners is same as that of the optimized designs in Table 2 and Table 3 ($\frac{2\times30.26\%}{1+2\times30.26\%}=37.70\%$). Moreover, the minimum size constraint is set as 2 mm, and the maximum size constraints are set as 5 mm, 10 mm, 15 mm, 20 mm, 25 mm, and 30 mm, respectively. The strain energy of optimized results and corresponding deformation fields with different maximum size control parameters are listed in Table 5.

Table 5 The optimized results and corresponding deformation fields by topology optimization with Demold constraint and different size controls

Maximum size control parameter [mm]	*Strain energy* [J]	Deformation fields
5.00	1158.89	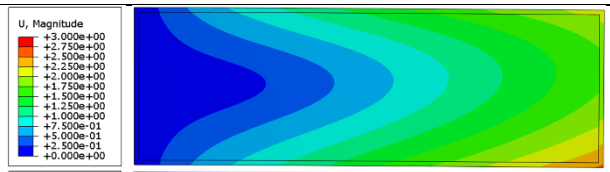
10.00	863.16	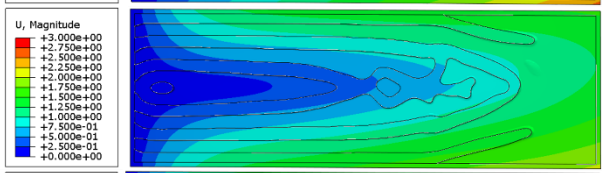
15.00	856.35	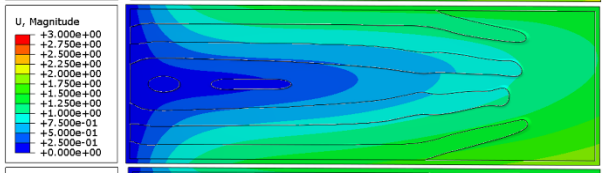
20.00	844.39	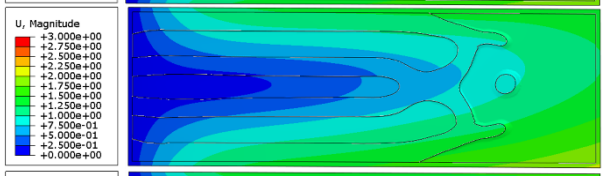
25.00	842.73	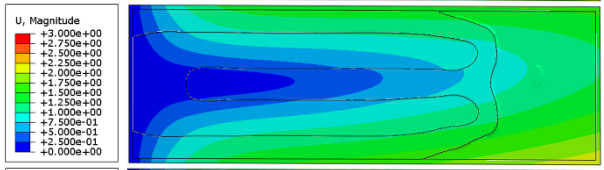
30.00	834.66	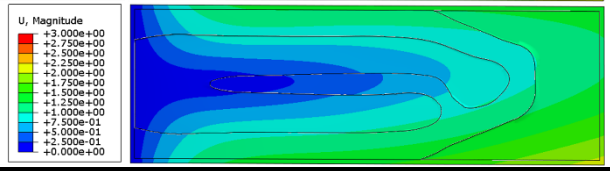

Obviously, the optimized stiffener design by the proposed method is better than the result obtained by SIMP topology optimization from the perspective of deformation mode. Moreover, it can be seen that there are intermittent stiffeners in the SIMP optimized result. This does not meet the design requirements of continuous stiffeners that are common in engineering stiffened thin-walled structures. Besides, the stiffeners do not extend from one side to the other side. There are even cases where a clear stiffener path cannot be obtained and the size control failed. Especially when the volume fraction is ultra-low, it is more challenging to optimize continuous and clear stiffener paths. These are the tough problems that the traditional topology optimization faces in the design of stiffener path layouts. In contrast, the GDMSP can efficiently and robustly obtain

continuous and clear stiffener paths, which can be directly used for detailed modeling and structural size optimization. The GDMSP can change the topology and realize the optimal ratio of stiffness distribution of the structure by optimizing the stiffener layout. Furthermore, the concurrent optimization of the layout variable (the number of seed points) and size variables can achieve the optimization design with a given mass constraint. In addition, it is suggested that the size of the fixed mesh should be small in the step of stiffener layout topology optimization. Then, the number of stiffeners can be changed by changing the layout variable in the step of structural size design, thereby changing the mass of the structure. In this way, it is not needed to re-execute the stiffener layout topology optimization when changing the mass constraint and the mesh size in DMO. Overall, the proposed GDMSP can robustly provide a distinct stiffener layout, and the optimized design has a significant stiffness improvement compared to the traditional design.

4. Buckling load maximization of square stiffener plate with the non-uniform sinusoidal load

In this section, buckling load maximization optimization for a square stiffener plate is carried out. The length of the square plate *l* is 1000 mm. The material is the same as that in section 3, and the mesh is fixed with 400 (20×20) elements. The left and the right boundaries are fixed in *z* and θ_y, the bottom left vertex fixed in *y* and the bottom right vertex is fixed in *x* and *y*. The square plate is subjected to the non-uniform axial load. Specifically, 1 N/mm uniform distributed loads are applied on the top edge and lower edge, respectively. Non-uniform sinusoidal loads are applied on the left edge and right edge, which are expressed in Eq.(19), as shown in Fig. 12.

$$\begin{aligned} F_{left} &= \sin(3\pi \frac{y}{l}) + 1 \\ F_{right} &= -2\sin(2\pi \frac{y}{l} + \frac{\pi}{4}) + 1 \end{aligned} \tag{19}$$

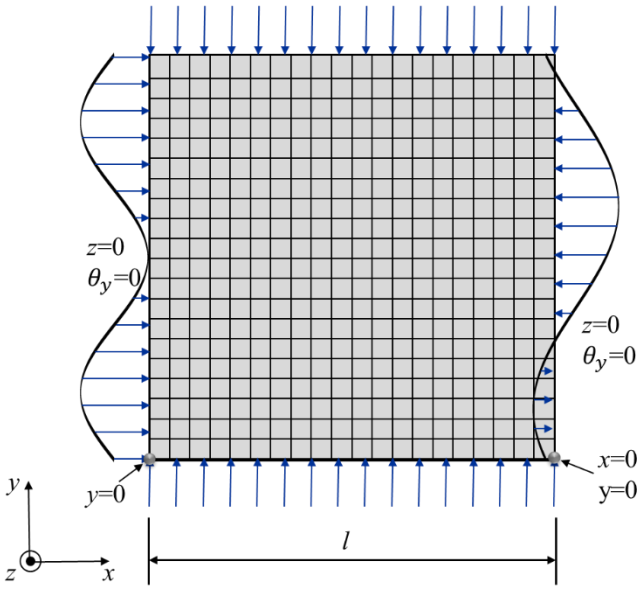

Fig. 12 Schematic diagram of a square plate with mesh, boundary and the non-uniform sinusoidal load

The sizes of the stiffener cell introduced in section 3 are enlarged ten times, i.e., the length of the stiffener cell becomes 50 mm, and the corresponding stiffness coefficients are listed in Table 6. The DMO is then used to optimize the stiffener layout. The optimization objective is to maximize the buckling load factor, where the optimization parameters are the same as those in section 3, and sensitivities are calculated with the adjoint method as Eq.(28) in the appendix. The optimization formula is as Eq.(20).

Table 6 The equivalent general stiffness coefficients of the stiffener cell with 50 mm length

A_{11}	A_{12}	A_{13}	A_{21}	A_{22}	A_{23}	A_{31}	A_{32}	A_{33}
1.37e6	2.76e5	-1.43e-8	2.76e5	1.37e6	-1.30e-8	-1.47e-8	-1.30e-8	3.04e5
B_{11}	B_{12}	B_{13}	B_{21}	B_{22}	B_{23}	B_{31}	B_{32}	B_{33}
-4.00e7	-1.00e7	3.06e-7	-1.00e7	-4.00e7	-4.27e-7	1.89e-7	4.11e-7	-1.16e7
D_{11}	D_{12}	D_{13}	D_{21}	D_{22}	D_{23}	D_{31}	D_{32}	D_{33}
1.46e9	3.92e8	-1.47e-5	3.92e8	1.46e9	-2.84e-5	-1.54e-5	-2.59e-5	4.61e8

$$\begin{aligned} &\max_{\boldsymbol{x}} : P \\ &\text{subject to}: P = \min(\lambda_j), \quad j = 1,...,n_{dof} \\ &\qquad \{\mathbf{K} + \lambda_j \mathbf{K}_\sigma\}\boldsymbol{\Phi}_j = \mathbf{0} \\ &\qquad 0.0 \le \underline{x} \le x_{ij} \le 1.0, \quad i = 1,...,n, \quad j = 1,...,m \end{aligned} \tag{20}$$

where P is the buckling load, $\mathbf{K}_\sigma$ is the global geometric stiffness matrix, n_{dof} is the number of degrees of freedom, λ_j is the jth eigenvalue, and $\mathbf{\Phi}_j$ is the corresponding eigenvector. Then, the optimized discrete angles distribution of stiffener cells can be obtained by DMO. It is seen that the distribution of angles can be divided into five parts from the horizontal direction, as shown in Fig. 13. The first, third and fifth parts are mainly 0 degrees because they bear the main axial load on four edges, respectively. The second and fourth parts are mainly 45 degrees because they mainly play the role of force transmission.

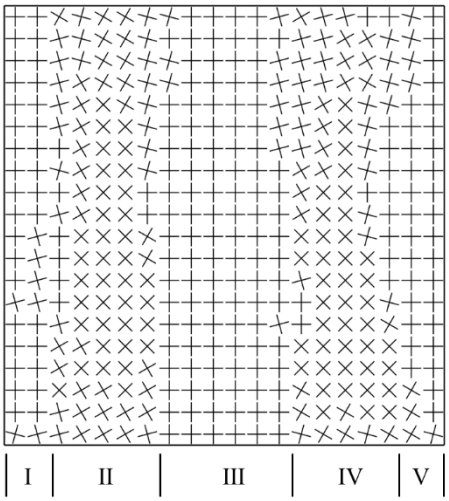

Fig. 13 The discrete angle distribution of stiffener cells obtained by DMO for buckling optimization of the square stiffener plate

For this example, the manufacturing techniques are considered. In engineering, curved stiffeners are not easy to manufacture and straight stiffeners are available. Therefore, the curve path of stiffeners is further extracted, categorized, and features simplified to the straight stiffener path, and the uniform stiffener layout is adopted, as shown in Fig. 14, where the primary trend of the angle gradient is retained.

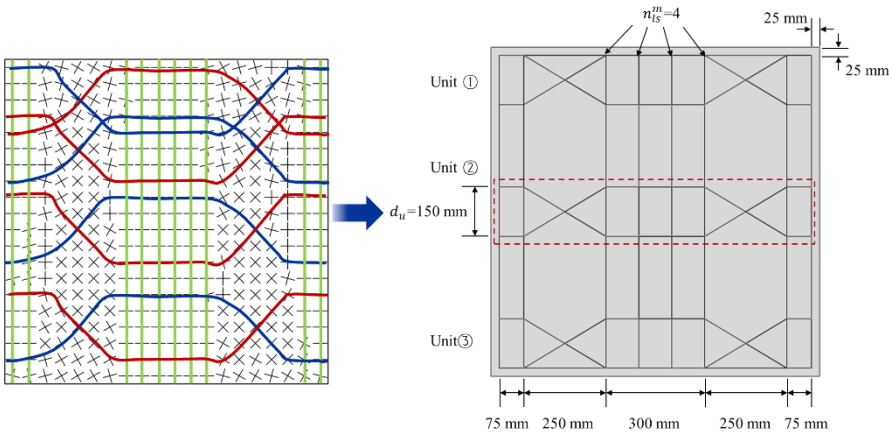

Fig. 14 The feature-simplified straight stiffener path extracted from the optimized stiffener configuration for buckling optimization of the square stiffener plate

Structural size optimizations of the optimized configuration design and the traditional orthogonal configuration are performed. For the optimized configuration, the number of units n_u, the number of longitudinal stiffeners n_{ls}^{m} in the middle area, and the distance between two stiffeners in the unit d_u are set as the layout variables, the height of stiffeners $h_{stiffener}$, the thickness of stiffeners $t_{stiffener}$, and the thickness of skin t_{skin} are set as size variables during the detailed optimization process. For the design of traditional orthogonal stiffener configuration, the types of variables are the same as those in section 3. The formula of the maximization buckling load of buckling load with mass constraint is as follows,

$$\begin{aligned} &\max_{X} : P \\ &\text{subject to}: P = \min(\lambda_j), \quad j = 1,...,n_{dof} \\ &\{\mathbf{K} + \lambda_j \mathbf{K}_\sigma\}\mathbf{\Phi}_j = \mathbf{0} \\ &M \le \overline{M} \\ &\underline{X_d} \le X_d \le \overline{X_d} \\ &\underline{X_c} \le X_c \le \overline{X_c} \end{aligned} \tag{21}$$

The structure is modeled with the S3 3D shell element in ABAQUS, the mesh size is 5 mm, and the linear buckling load is obtained by the Lanczos algorithm. The hybrid optimization strategy is used, and the optimization parameters are the same as that in section 3.2. For the optimized configuration, a total of 8090 analyses based on detailed finite element models are performed, which takes about 374 hours. After the hybrid optimization, the optimized parameters and buckling load factors are shown in Table 7 and Table 8. Moreover,

the buckling modes of optimized results are shown in Fig. 15.

Table 7 The upper limits, the lower limits, the mass constraint and optimized design parameters of variables of the optimized stiffener layout design for maximization buckling load

	n_u	n_{ls}^m	d_u [mm]	t_{skin} [mm]	$h_{stiffener}$ [mm]	$t_{stiffener}$ [mm]	M [kg]	Buckling load factor
Lower limit of variables	1	2	50.00	2.20	11.00	1.30	-	-
Upper limit of variables	30	30	300.00	3.00	16.00	1.90	8.00	-
Optimized design parameters	10	3	147.00	2.20	16.00	1.69	8.00	**21.4**

Table 8 The upper limits, the lower limits, the mass constraint and optimized design parameters of variables of the traditional orthogonal configuration for maximization buckling load

	n_{ts}	n_{ls}	t_{skin} [mm]	$h_{stiffener}$ [mm]	$t_{stiffener}$ [mm]	M [kg]	Buckling load factor
Lower limit of variables	2	2	2.20	11.00	1.30	-	-
Upper limit of variables	50	50	3.00	16.00	1.90	8.00	-
Optimized design parameters	20	15	2.20	16.00	1.43	8.00	15.8

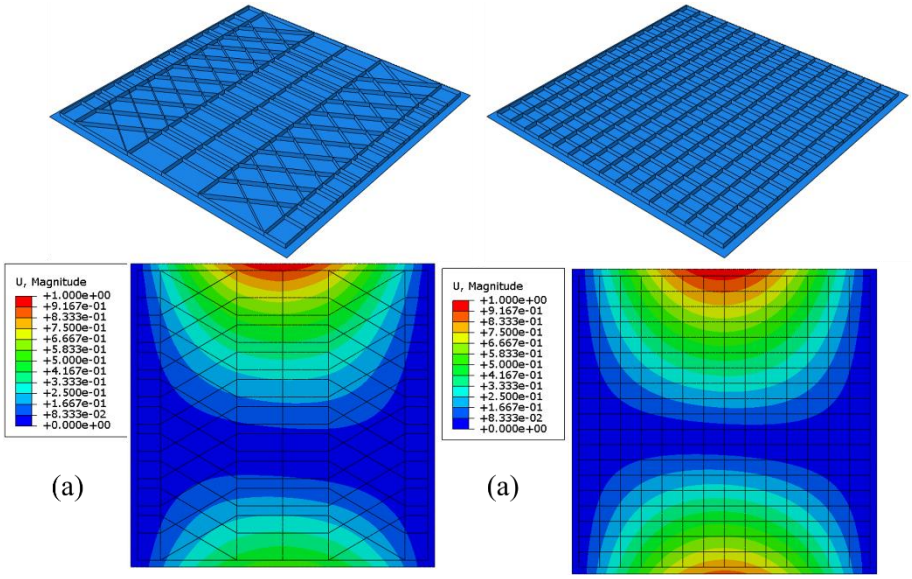

Fig. 15 The structure models after the structural size optimization and corresponding deformation fields under the non-uniform sinusoidal load, (a) the optimized stiffener layout design, (b) the traditional orthogonal configuration stiffener design

The buckling load factor of the optimized design is 35.44% higher than that of the traditional orthogonal design. For the last design, the mass of stiffeners is 2.06 kg, and the mass of the skin is 5.94 kg. If similar

solutions tend to be obtained by topology optimization with Demold constraint, the volume constraint should be 4.77%. Moreover, it is found that the height of stiffeners all reach the upper limit of bounds. It is demonstrated that the stiffener height has a significant effect on the buckling load, which increases the bending stiffness of the structure. Besides, it is crucial that the novel design is composed of uniform and straight stiffeners, which does not challenge the existing manufacturing technology. Even with the complex non-uniform loads, the buckling load of structures can be significantly improved only by optimizing the stiffener topology layout. Overall, the GDMSP can also efficiently solve the stiffener layout optimization of buckling load and can provide a design that improves the buckling load and satisfies the manufacturing technology at the same time.

5. Conclusions

In this paper, a generative design method of stiffened plates (GDMSP) based on the homogenization method is established. It can optimize the stiffener topology layout based on an equivalent model. A detailed model can then be obtained by extracting the stiffener path from the discrete distribution of stiffener angles. Moreover, the optimized design can be obtained by structural size optimization based on the detailed model. In order to illustrate the GDMSP and verify its effectiveness, two examples are presented. The first one is the stiffness maximization of the rectangle stiffener plate with a distributed load. For this example, the stiffener path is characterized by streamlines, and the optimized design after the structural size optimization has an improvement of 17% compared with the traditional orthogonal configuration design. The second one is the buckling load maximization of the square stiffener plate with the non-uniform sinusoidal load. For this example, the curve path of stiffeners is further extracted, categorized, and features simplified to the straight path, and the non-uniform layout is transformed into the uniform layout. Finally, the design improves the buckling load by 35% and satisfies the manufacturing technology at the same time. Overall, the proposed GDMSP can effectively improve the performance of the structure by changing the stiffener topology layout compared with the traditional configuration design and provide a novel and clear stiffener path, which can be directly used to establish the detailed numerical model. Besides, it should be noted that there may be some problems in the extraction of the stiffener path for the non-convex design domain with cutouts due to the discontinuity of angle distribution, which will continue to be investigated in the following work.

Appendix: the sensitivity analysis of the linear buckling load

In this paper, the linear buckling load is calculated with the finite element method by solving the eigenvalue equation as follows.

$$\{\mathbf{K}+\lambda_j\mathbf{K}_\sigma\}\mathbf{\Phi}_j=\mathbf{0} \tag{22}$$

For the DMO, the sensitivities are necessary. The sensitivities are calculated with the adjoint method, which is briefly derived as follows. The direct approach to obtain the eigenvalue sensitivity in case of a distinct, i.e., the simple eigenvalue λ_j is to differentiate Eq.(22) to the design variable x_{ij} premultiply by $\mathbf{\Phi}_j^T$ and make use of Eq.(22). Then the following expression can be obtained as

$$\frac{d\lambda_j}{dx_{ij}}=-\mathbf{\Phi}_j^T\left(\frac{d\mathbf{K}}{dx_{ij}}+\lambda_j\frac{d\mathbf{K}_\sigma}{dx_{ij}}\right)\mathbf{\Phi}_j \tag{23}$$

where it has been assumed that the eigenvectors have been $\mathbf{K}_\sigma$ -orthonormalized, such that $\mathbf{\Phi}_i^T\mathbf{K}_\sigma\mathbf{\Phi}_i=1$. The geometric matrix is an implicit function of the displacement field, i.e. $\mathbf{K}_\sigma=\mathbf{K}_\sigma\left(\mathbf{u(x)},\mathbf{x}\right)$, which have to be taken into account as

$$\frac{d\mathbf{K}_\sigma}{dx_{ij}}=\frac{\partial\mathbf{K}_\sigma}{\partial x_{ij}}+\frac{\partial\mathbf{K}_\sigma}{\partial\mathbf{u}}\frac{d\mathbf{u}}{dx_{ij}} \tag{24}$$

Then the static equilibrium equation $\mathbf{Ku}=\mathbf{F}$ is differentiated to the design variable x_{ij} as

$$\mathbf{K}\frac{d\mathbf{u}}{dx_{ij}}=\frac{\partial\mathbf{F}}{\partial x_{ij}}-\frac{\partial\mathbf{K}}{\partial x_{ij}}\mathbf{u} \tag{25}$$

where the load sensitivity $\partial\mathbf{F}/\partial x_{ij}$ is zeros. Then, substituting Eq.(25) into Eq.(24) yields

$$\frac{d\mathbf{K}_\sigma}{dx_{ij}}=\frac{\partial\mathbf{K}_\sigma}{\partial x_{ij}}-\frac{\partial\mathbf{K}_\sigma}{\partial\mathbf{u}}\mathbf{K}^{-1}\frac{d\mathbf{K}}{dx_{ij}}\mathbf{u} \tag{26}$$

Thus, the adjoint vector $\mathbf{\Lambda}$ that satisfies the Eq.(27) can be introduced.

$$\mathbf{K\Lambda}=\left(\mathbf{\Phi}_j^T\frac{\partial\mathbf{K}_\sigma}{\partial\mathbf{u}}\mathbf{\Phi}_j\right)^T \tag{27}$$

Finally, substituting the adjoint vector $\mathbf{\Lambda}$ into Eq.(23), the full-analytically design sensitivities can be obtained as follow.

$$\frac{d\lambda_j}{dx_{ij}}=-\left(\mathbf{\Phi}_j^T\frac{d\mathbf{K}}{dx_{ij}}\mathbf{\Phi}_j+\lambda_j\mathbf{\Phi}_j^T\frac{\partial\mathbf{K}_\sigma}{\partial x_{ij}}\mathbf{\Phi}_j-\lambda_j\mathbf{\Lambda}^T\frac{d\mathbf{K}}{dx_{ij}}\mathbf{u}\right) \tag{28}$$

Acknowledgments

This study was funded by the National Natural Science Foundation of China (11772078 and 11825202), the Project supported by Liaoning Provincial Natural Science Foundation (2019-YQ-01), Liaoning Revitalization Talents Program (XLYC1907142 and XLYC1802020). Moreover, the authors gratefully acknowledge financial support from the China Scholarship Council.

Compliance with ethical standards

Conflict of interest The authors declare that they have no conflict of interest.

Replication of results All the key formulas for the calculation have been provided in the article. If the reader is interested, we can provide the Matlab code.

References

[1] Cheng K-T, Olhoff N. An investigation concerning optimal design of solid elastic plates. Int J Solids Struct 1981;17:305–23.

[2] Chung J, Lee K. Optimal design of rib structures using the topology optimization technique. Proc Inst Mech Eng -- Part C 1997;211:425–37.

[3] Zhou M, Fleury R, Shyy Y-K, Thomas H, Brennan J. Progress in Topology Optimization with Manufacturing Constraints. 9th AIAA/ISSMO Symp. Multidiscip. Anal. Optim., American Institute of Aeronautics and Astronautics; 2002.

[4] Lam YC, Santhikumar S. Automated rib location and optimization for plate structures. Struct Multidiscip Optim 2003;25:35–45. doi:10.1007/s00158-002-0270-7.

[5] Gersborg AR, Andreasen CS. An explicit parameterization for casting constraints in gradient driven topology optimization. Struct Multidiscip Optim 2011;44:875–81.

[6] Zhu J-H, Gu X-J, Zhang W-H, Beckers P. Structural design of aircraft skin stretch-forming die using topology optimization. J Comput Appl Math 2013;246:278–88.

[7] Liu S, Li Q, Chen W, Hu R, Tong L. H-DGTP—a Heaviside-function based directional growth topology parameterization for design optimization of stiffener layout and height of thin-walled structures. Struct Multidiscip Optim 2015;52:903–13.

[8] Zhang S, Norato JA, Gain AL, Lyu N. A geometry projection method for the topology optimization of plate structures. Struct Multidiscip Optim 2016;54:1173–90. doi:10.1007/s00158-016-1466-6.

[9] Zhang S, Gain AL, Norato JA. Adaptive mesh refinement for topology optimization with discrete geometric components. Comput Methods Appl Mech Eng 2020;364:112930. doi:https://doi.org/10.1016/j.cma.2020.112930.

[10] Zhang S, Norato JA. Optimal Design of Panel Reinforcements With Ribs Made of Plates. J Mech Des 2017;139. doi:10.1115/1.4036999.

[11] Wang B, Zhou Y, Tian K, Wang G. Novel implementation of extrusion constraint in topology optimization by Helmholtz-type anisotropic filter. Struct Multidiscip Optim 2020.

[12] Aage N, Andreassen E, Lazarov BS, Sigmund O. Giga-voxel computational morphogenesis for structural design. Nature 2017;550:84.

[13] Oberndorfer JM, Achtziger W, Hörnlein HREM. Two approaches for truss topology optimization: a comparison for practical use. Struct Optim 1996;11:137–44.
[14] Ding X, Yamazaki K. Stiffener layout design for plate structures by growing and branching tree model (application to vibration-proof design). Struct Multidiscip Optim 2004;26:99–110.
[15] Ji J, Ding X, Xiong M. Optimal stiffener layout of plate/shell structures by bionic growth method. Comput Struct 2014;135:88–99. doi:https://doi.org/10.1016/j.compstruc.2014.01.022.
[16] Hu T, Ding X, Shen L, Zhang H. Improved adaptive growth method of stiffeners for three-dimensional box structures with respect to natural frequencies. Comput Struct 2020;239:106330. doi:https://doi.org/10.1016/j.compstruc.2020.106330.
[17] Liu H, Li B, Yang Z, Hong J. Topology optimization of stiffened plate/shell structures based on adaptive morphogenesis algorithm. J Manuf Syst 2017;43:375–84. doi:https://doi.org/10.1016/j.jmsy.2017.02.002.
[18] Zhou Y, Tian K, Xu S, Wang B. Two-scale buckling topology optimization for grid-stiffened cylindrical shells. Thin-Walled Struct 2020;151:106725. doi:https://doi.org/10.1016/j.tws.2020.106725.
[19] Sun Z, Cui R, Cui T, Liu C, Shi S, Guo X. An Optimization Approach for Stiffener Layout of Composite Stiffened Panels Based on Moving Morphable Components (MMCs). Acta Mech Solida Sin 2020.
[20] Lazarov BS, Wang F. Maximum length scale in density based topology optimization. Comput Methods Appl Mech Eng 2017;318:826–44.
[21] Hao P, Wang B, Tian K, Li G, Du K, Niu F. Efficient Optimization of Cylindrical Stiffened Shells with Reinforced Cutouts by Curvilinear Stiffeners. AIAA J 2016;54:1–14.
[22] Hirschler T, Bouclier R, Duval A, Elguedj T, Morlier J. The embedded isogeometric Kirchhoff–Love shell: From design to shape optimization of non-conforming stiffened multipatch structures. Comput Methods Appl Mech Eng 2019;349:774–97.
[23] Wang D, Abdalla MM, Zhang W. Sensitivity analysis for optimization design of non-uniform curved grid-stiffened composite (NCGC) structures. Compos Struct 2018;193:224–36.
[24] Kegl M, Brank B. Shape optimization of truss-stiffened shell structures with variable thickness. Comput Methods Appl Mech Eng 2006;195:2611–34. doi:https://doi.org/10.1016/j.cma.2005.05.020.
[25] Zhao W, Kapania RK. Buckling analysis of unitized curvilinearly stiffened composite panels. Compos Struct 2016;135:365–82.
[26] Wang D, Abdalla MM, Wang Z-P, Su Z. Streamline stiffener path optimization (SSPO) for embedded stiffener layout design of non-uniform curved grid-stiffened composite (NCGC) structures. Comput Methods Appl Mech Eng 2019;344:1021–50.
[27] Wang D, Yeo S-Y, Su Z, Wang Z-P, Abdalla MM. Data-driven streamline stiffener path optimization (SSPO) for sparse stiffener layout design of non-uniform curved grid-stiffened composite (NCGC) structures. Comput Methods Appl Mech Eng 2020;365:113001.
[28] Liu D, Hao P, Zhang K, Tian K, Wang B, Li G, et al. On the integrated design of curvilinearly grid-stiffened panel with non-uniform distribution and variable stiffener profile. Mater Des 2020;190:108556.
[29] Hao P, Wang Y, Liu C, Wang B, Tian K, Li G, et al. Hierarchical Nondeterministic Optimization of Curvilinearly Stiffened Panel with Multicutouts. AIAA J 2018;56:1–15.
[30] Slemp WCH, Bird RK, Kapania RK, Havens D, Norris A, Olliffe R. Design, Optimization, and Evaluation of Integrally Stiffened Al-7050 Panel with Curved Stiffeners. J Aircr 2011;48:1163–75.
[31] Liu Y, Shimoda M. Non-parametric shape optimization method for natural vibration design of stiffened shells. Comput Struct 2015;146:20–31.
[32] Bojczuk D, Szteleblak W. Optimization of layout and shape of stiffeners in 2D structures. Comput Struct 2008;86:1436–46.
[33] Jármai K, Snyman JA, Farkas J. Minimum cost design of a welded orthogonally stiffened cylindrical shell. Comput Struct 2006;84:787–97.
[34] Bushnell D. Optimization of composite, stiffened, imperfect panels under combined loads for service in the postbuckling regime. Comput Methods Appl Mech Eng 1993;103:43–114. doi:https://doi.org/10.1016/0045-7825(93)90041-U.
[35] Tian K, Wang B, Zhang K, Zhang J, Hao P, Wu Y. Tailoring the optimal load-carrying efficiency of

hierarchical stiffened shells by competitive sampling. Thin-Walled Struct 2018;133:216–25.
[36] Wang B, Tian K, Zhou C, Hao P, Zheng Y, Ma Y, et al. Grid-pattern optimization framework of novel hierarchical stiffened shells allowing for imperfection sensitivity. Aerosp Sci Technol 2017;62:114–21.
[37] Hao P, Wang B, Tian K, Li G, Sun Y, Zhou C. Fast procedure for Non-uniform optimum design of stiffened shells under buckling constraint. Struct Multidiscip Optim 2017;55:1503–16.
[38] Ansola R, Canales J, Tárrago JA, Rasmussen J. An integrated approach for shape and topology optimization of shell structures. Comput Struct 2002;80:449–58. doi:https://doi.org/10.1016/S0045-7949(02)00019-6.
[39] Cheng G-DD, Cai Y-WW, Xu L. Novel implementation of homogenization method to predict effective properties of periodic materials. Acta Mech Sin 2013;29:550–6.
[40] Cai Y, Xu L, Cheng G. Novel numerical implementation of asymptotic homogenization method for periodic plate structures. Int J Solids Struct 2014;51:284–92.
[41] Lund E. Buckling topology optimization of laminated multi-material composite shell structures. Steel Constr 2009;91:158–67.
[42] Stegmann J, Lund E. Discrete material optimization of general composite shell structures. Int J Numer Methods Eng 2005;62:2009–27.
[43] Lund E, Stegmann J. On structural optimization of composite shell structures using a discrete constitutive parametrization. Wind Energy 2010;8:109–24.
[44] Bruyneel M. SFP--a new parameterization based on shape functions for optimal material selection: application to conventional composite plies. Struct Multidiscip Optim 2011;43:17–27.
[45] Gao T, Zhang W, Pierre D. A bi-value coding parameterization scheme for the discrete optimal orientation design of the composite laminate. Int J Numer Methods Eng 2012;91(1):98-114.
[46] Svanberg K. The method of moving asymptotes—a new method for structural optimization. Int J Numer Methods Eng 2010;24:359–73.
[47] Yan J, Duan Z, Lund E, Wang J. Concurrent multi-scale design optimization of composite frames with manufacturing constraints. Struct Multidiscip Optim 2017;56:519–33. doi:10.1007/s00158-017-1750-0.
[48] Miki Man & Cybernetics Conference Smc MBT-IS. A parallel genetic algorithm with distributed environment scheme, 1999.
[49] Schittkowski K. NLPQL: A FORTRAN subroutine for solving constrained nonlinear programming problems. Ann Oper Res 1986;5:485–500.
[50] Yan J, Cheng G, Liu L. A Uniform Optimum Material Based Model for Concurrent Optimization of Thermoelastic Structures and Materials. Int J Simul Multidisci Des Optim 2008;2:259–66.
[43] ABAQUS Standard User's Manual Version 6.10[M]. Pawtucket: Karlsson and Sorensen Inc., 2010.